Effect of fullerene content on the thermal, microstructure, and electrokinetic properties of fullerene/poly(vinyl pyrrolidone) nanofluids and nanocomposites

M. Behera

Silicon Institute of Technology, Bhubaneswar-751 024, India
email: mano.silicon@gmail.com

Abstract

In this study I report the thermal stability, microstructures, dynamic light scattering (DLS) and electro-kinetic effect in the fullerene (C_{60}):poly(vinyl pyrrolidone) PVP nanofluids (NFs) and nanocomposite films. An improvement in the degradation temperature of C_{60}:PVP nanocomposite reported here is ascribed to free radical scavenging ability of C_{60}. An analysis of DLS data in terms of polydispersity index (PDI) reveals a well dispersed structure of C_{60} assemblies with PVP in liquid medium. The typical electro-kinetic parameters such as zetapotential (ξ) and surface conductivity (σ_{sc}) in a NF evaluates the magnitude of electrostatic repulsion between C_{60} particles and such measurement tender a way to boost stability of C_{60} nanoparticles in presence of PVP molecules in a particular carrier. Microstructures in various films were found to vary with increasing in the C_{60} content and decreasing in the relative PVP content in the nanocomposites. Highest thermal degradation temperature (~ 422 ^{0}C) was observed for the sample consisting of 13.9 μM C_{60} owing to uniform distribution of C_{60} in the PVP matrix with a low PDI (0.272).

1. Introduction

Thermal degradation of raw macromolecular compounds at the early stage is a major setback to polymer industry [1,2]. In recent years many studies have been focused on improving their thermal stability by introducing nanofillers into the host matrix by both physical and chemical processes [3-8]. Miniscule fillers mostly used in improving the thermal properties of polymers could be clay, metal nanoparticles (NPs), metal oxides, carbon nanotube, and fullerene (C_{60}). Although many mechanisms have been proposed to explain enhancement in thermal properties of polymer nanocomposites upon introduction of NPs, the radical trapping of free radicals believe to be suite the most. Among the various classes of nanofillers, C_{60} is one of the most widely noticed filling agents because of its high reactivity towards free radicals [5-12] In an article [12], it reported that uniform dispersion of Pd NPs in the polymer matrix increases the thermal decomposition temperature of polypropylene (PP), polystryrene (PS) and polymethyl methacrylate (PMMA).

A three dimensional free radical scavenger like C_{60} has been reported by authors that it improves the thermal stability of various polymers [5-12]. In an article, Zhao et al. [5] reported that the resistance to the thermal degradation of high density polyethylene, PP, PMMA, and bisphenol-A polycarbonate were improved a lot with the addition of C_{60}. Their results showed that the influences of C_{60} on the resistance to the thermal degradation of different polymers were dependent on radical trapping thermal degradation mechanism. The influence of C_{60} on the thermal degradation of PMMA and polyvinyl chloride (PVC) is connected with its interruption of a chain radical reaction of the thermal degradation of PVC and PMMA. Gaspar et al. [6] have compared with pure PMMA, both C_{60} and PCBM increase substantially the thermal degradation temperature of the corresponding composites, both in nitrogen and air atmospheres. It is

reported by Katiyar et al. [7] that incorporation of C_{60} in the PMMA increases the both onset temperature of polymer degradation/decomposition and temperature of maximum weight loss only because of radical scavenging effect of $C_{60.}$ The impact of two different fullerenes (C_{60} and a functionalized C_{60}) on the thermal stability of the corresponding polystyrene (PS)-fullerene composites was studied by Fernandes et al. [8] using dynamic thermo gravimetric analysis. According to them the improved thermo-oxidative stability of the functionalized-fullerene composites compared to the C_{60} composites is due to the fact that former disperses better in a PS matrix than C_{60}.The results showed that the influence of C_{60} to resist early thermal degradation of different polymers were dependent on their degradation mechanism. The resistance to the thermal degradation of many polymers such as HDPE, PP, and PMMA were improved with the addition of C_{60} indicated that the radical trapping route played a dominant role. Kukobo et al. [9] have reported that the thermo-oxidative stability of PMMA/C_{60} nanocomposite with optimal loading (0.4–0.8 wt% C_{60}) exhibited larger thermal stability over PMMA. They attributed this enhancement to the radical-scavenging ability of π-conjugative fullerenes. In another article, Song et al. [10] studied the influence of C_{60} on the thermal properties of PP and found that C_{60} improved the thermal properties of PP by trapping free radicals and in situ forming a gelled-ball crosslink network. Zuev et al. [11] studied that the influence of C_{60} on the thermal behavior and thermo-degradation of acrylic polymers. The results showed that the decomposition process of acrylic polymers changed from a radical pathway to a non-radical pathway with the addition of C_{60}.

In nano-systesms, since the strong van der Waals interactions between small structures always favor aggregation and afterward sedimentation, developing a stable nanofluid (NF) is not an easy task for the chemists. In general, stability in a NF comes as a result of interplay of the heat (kinetic) energy of the flocculates, attractive forces between the flocculates, and repulsive forces between the flocculates and the liquid carrier. It is reported that, particles with zetapotential (ξ) ≥ (±) 30 mV are normally considered as stable in a suspension [13,14]. The electrostatic stabilization of small structures in a suspension is successfully described by the DLVO theory, named after the work of Derjaguin, Landau, Verwey, and Overbeek [13,14]. In an experiment, Rahme et al. [15] found that the ξ-value in a NF also depends on the host structure. A ξ-value had been decreased from (-) 35 mV to (-) 1 mV in a gold reinforced polyethylene glycol (PEG) NF in a nonlinear path when PEG molecular weight was increased from 2,100 to 51,400 g mol^{-1}. They remarked that such a decrease in the ξ-value with an increased molecular weight of a liquid carrier is not surprising as zeta potential is measured at the surface plane of the hydrodynamic sphere of diameter and the surface plane of the hydrodynamic sphere is far from the surface of flocculates in a stable NF.

The dynamic light scattering (DLS) is a technique which is capable of measuring average size of flocculates like C_{60} clusters in terms of (L_{hd}) and width of distribution as polydispersity index (PDI) in a NF [13,16.17]. In DLS, the speed at which the nanoparticles (NPs) are diffusing in a NF due to the Brownian motion over a liquid carrier is measured very precisely. As the NPs in a NF are under constant, but random Brownian motion, they cause the intensity of scattered light from them to fluctuate as a function of time. In general, the small particles cause the intensity to fluctuate more rapidly than effectively larger ones. So, the L_{hd}-value of C_{60} in a NF can be obtained from the temporal autocorrelation function relative to the diffused light intensity. From the literatures [13,14], the hydrodynamic diameter L_{hd}-value is obtained from a field correlation function $g^1(\tau)$ which is an exponential decaying function of a correlator time delay τ;

$$g^1(\tau) = A[1 + \beta \exp(-2\Gamma\tau)], \quad (1)$$

where A is a base line, β is an intercept of the correlation function, which represents the degree of spatial coherence of the scattered light over the detector, and it is determined by the ratio of the detector area to the area of one speckle ($0 < \beta < 1$), while $\Gamma = Dq^2$ describes the particle relaxation with an autocorrelation time τ (= $1/\Gamma$) and a translational diffusion coefficient D. The τ-value gives information about a dynamic fluid behavior. The scattering wavevector, $q = (4\pi\mu/\lambda) \sin(\theta/2)$, is determined by the refractive index μ of the medium, wavelength of laser λ and the scattering angle θ. For model spherical particles, the D_0 value (D =

D_0 at infinite dilution of a fluid) relates to the effective L_{hd} value in a well-known Stokes-Einstein relation [16,17]:

$$D_0 = kT/3\pi\eta L_{hd}, \quad (2)$$

which yields the L_{hd}-value at temperature T after putting the viscosity (η) of the solvent and the Boltzmann constant $k = 1.38 \times 10^{-23}$ JK^{-1}.

Alagrova et al. [18] studied the variation of $g^1(\tau)$ against decay time for a colloidal dispersion of C_{60} in a toluene/acetonitrile mixture solution in absence of stabilizing agent. As they have reported, a PDI of 0.1 appears from a second-order cumulant fit analysis. In another experiment, Chaudhari et al. [19] studied the variation of electric field correlation function of 50 mM sodium dodecyl sulfate surfactant (SDS) at different anilium nitrate (AN) concentrations. They reported that relaxation time of $g^1(\tau)$ increases with increasing AN concentration due to an increase in effective size of the micelles and L_{hd}-value of SDS micelle has increased almost linearly with AN concentration in the micellar solution. There is a report by Mountrichas et al. [20] that both the PDI indices and average hydrodynamic diameters (L_{hd}) are increased upon increasing the C_{60}-content from 1–20 wt% in amphiphilic copolymer solubilized C_{60} in water. In C_{60}-polystyrene NFs in benzene, it is reported that the L_{hd}-value of C_{60} NPs decreases from 220 nm to 140 nm when concentration of the polymer has increased from 0.56 M to 2.5 M [21]. In another experiment, Rahme et al. [15) reported that L_{hd}-value of Au NPs has increased in a nonlinear way from 10 to 90 nm by increasing molecular weight of the polymer from 2,100 to 51,400 g mol^{-1} in grafted Au-PEG NFs in water due to a decrease in grafting density from 3.93 nm^2 to 0.32 nm^2. In Au-poly(acrylic acid) (PAA) NFs, it is reported that the L_{hd}-value of Au-NPs has decreased from 6.5 nm to 1.4 nm when the PAA content has increased from 0.006 mM to 6.0 mM in water [22]. In Au:PVP NFs in water, Mishra et al. [23] have reported a shift in the correlograms over larger L_{hd} values on increasing the Au-content from 2.54 to 50.76 mM, supporting a fact that a solid inclusion combine to PVP in joint assemblies. In an article on Au-PVA NFs, it is reported that with increase in the Au-content, the correlogram had shifted to right along the X-axis and that causes in delaying the time τ [24]. A comparison of all these above results implies that the structural parameters in a NF depends on several factors namely (i) initial size of the solid particles, (ii) interaction of the solid particles with the polymer additives if any used so that they form joint assemblies, and (iii) average concentration of the NF made in a particular liquid carrier.

In this article I discussed the thermal stability, the variation of degradation temperature, L_{hd}, PDI, ξ-value and surface conductivity (σ_{sc}) of PVP/C_{60} clusters present in the C_{60}:PVP NFs/nanocomposites of selective compositions with C_{60} content.

2.0 Synthesis of NFs and experimental measurements

99.9% purity C_{60} powder and K-25 grade PVP of average molecular weight of 28 kDa were purchased from Alfa Aesar and Aldrich chemicals, respectively. Toluene and n-butanol non-aqueous solvents of analytical grade were used to develop NFs. Getting information on the synthesis of C_{60}:PVP NFs in n-butanol, published article [25] may be referred. Thermo-Gravimetric analysis (TGA) was carried out using a TA Q500 thermo-balance. The instrument was calibrated with respect to indium and aluminum standards. Samples (~5 mg) were placed in alumina crucibles and dynamic tests were performed by heating the samples from 40 ^{0}C to 600 ^{0}C using a heating ramp of 10 ^{0}C min^{-1}, under nitrogen at 50 mL min^{-1}.The DLS experiments were carried out for the parent PVP solution and derived C_{60}:PVP NFs in *n*-butanol consisting of selective C_{60} content with the help of Malvern Nano Zetasizer Nano ZS instrument. An incident light beam was generated from a vertically polarized He-Ne laser beam of wavelength λ = 633.2 nm (of 4 mW power) fixed at one arm of a Goniometer. Before measuring the data, a NF was filtered through a 0.22 μm Teflon filter paper and loaded into a 3 mL quartz cell. The same instrument was also used to measure the electro-kinetic parameters of various NFs.

3.0 Results and discussion

3.1 DLS bands of C_{60}:PVP NFs

Figure 1 depicts the normalized $g^1(\tau)$ values measured for C_{60}:PVP NFs comprising (a) 0, (b) 4.63, (c) 9.26, (d) 13.9, (e) 18.52, and (f) 23.15 μM C_{60} along with 40.0 g/L PVP in *n*-butanol. A linear Γ dependence has been shown upon the q^2-value in describing $g^1(\tau)$ of a single (translational) diffusive relaxation mode. As it can be seen from the plot in Figure 1, with increase in the C_{60}- content, the correlogram hardly shifts along the X-axis. This reveals that a C_{60} doping barely influence the L_{hd}-value in a NF, and consequently has a little effect on the delay time τ. In general, if the C_{60} clusters are effectively large in size, the signal will change slowly and the correlation will persevere for a long time. If the particles are effectively small and moving rather rapidly, then correlation will reduce more quickly, and a correlogram will make a left-shift along the time-axis.

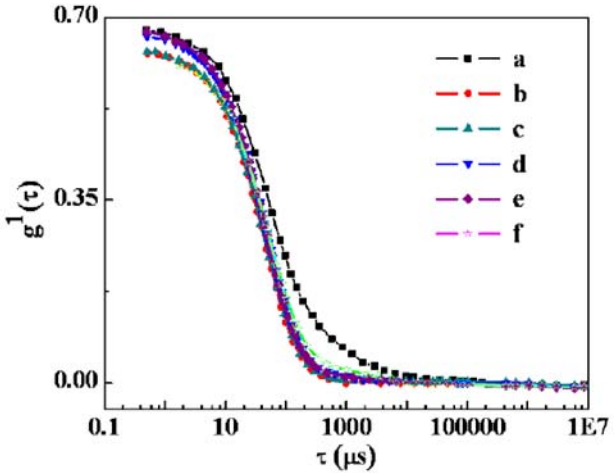

Figure 1. Variations of normalize $g^1(\tau)$ values against the time scale of measurement in C_{60}:PVP NFs in *n*-butanol; (a) 0, (b) 4.63, (c) 9.26, (d) 13.9, (e) 18.52, and (f) 23.15 μM C_{60}.

Further I studied DLS bands in the C_{60}:PVP NFs prepared with the different C_{60} dosages (a) 0, (b) 4.63, (c) 9.26, (d) 13.9, (e) 18.52, and (f) 23.15 μM in 40.0 g/L PVP in *n*-butanol. The experimental data could be collected over five times diluted samples which had an average 6.8 pH.

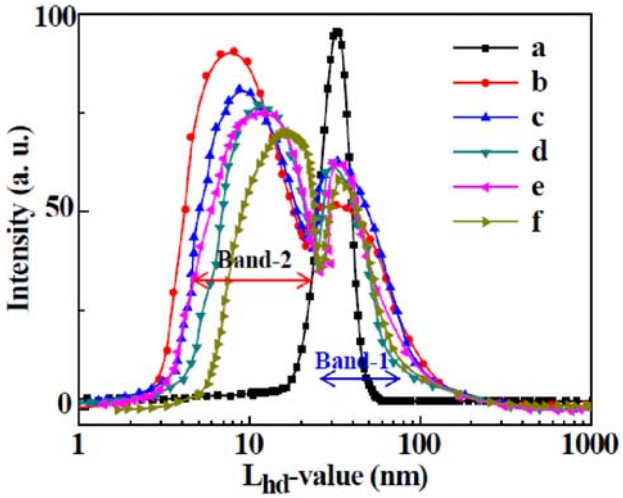

Figure 2. Distributions of L_{hd}-values in C_{60}:PVP NFs consisting of (a) 0, (b) 4.63, (c) 9.26, (d) 13.9, (e) 18.52, and (f) 23.15 μM C_{60} in 40.0 g/L PVP in *n*-butanol.

As it is can be seen from the DLS spectra portrayed in Figure 2, except the virgin sample (a) without having any C_{60} doping, all the C_{60}:PVP NFs exhibit two distinct DLS bands, indicating two types of size distributions of the flocculates. In sample (a) of only PVP molecules dispersed in *n*-butanol exhibits a single DLS band {full width at half maximum (fwhm) ~15.8 nm} with an average L_{hd}-value 30 nm and a PDI 0.298. It is observed that when only a small dosage of 4.63 μM C_{60} molecules is added to this sample, two well-separated bands split-up in two effective L_{hd}-values 32.0 and 8.1 nm. An average L_{hd}-value 9.2 nm is estimated from the total band profile, with PDI 0.35. The first Band-1 of 32.0 nm, which is reasonably broad (fwhm ~48.7 nm), attributes to PVP molecules dispersed in *n*-butanol. The Band-2 with fwhm ~15.9 nm arises in PVP-capped C_{60} particles. It is also examined from the plot that with an increase in the C_{60}-value, the average L_{hd}-value of Band-1 in the PVP molecules is almost unchanged whereas that has increased nonlinearly to as large as 17.0 nm in Band-2.

From the results in Table 1 for the various C_{60}:PVP NFs, a pretty small average L_{hd}-value 9.2 nm is found for a C_{60}:PVP NF, which consists of a reasonably small doping of 4.63 μM C_{60}, and that has grown-up significantly to 17.0 nm, i.e., nearly twice the above value upon increasing the doping dosage to 23.15 μM C_{60}. These results explicitly confer formation of relatively larger flocculates between the two kinds of the entities of PVP and C_{60} as a result that the C_{60} clusters and grows dispersed through PVP molecules which control the C_{60}:PVP clustering in a dispersed sample of a NF. Evidently, a PVP polymer solution not only acts as a C_{60} solubilizer in *n*-butanol, but also extends an excellent surface encapsulant so that it retards C_{60}:PVP clustering in small assemblies. Technically, this is highly required to produce a stable NF with functionalized properties.

Table 1: The values of ξ, σ_{sc}, L_{hd}, and PDI determined from zetapotential and DLS for PVP solution and synthesized C_{60}:PVP NFs in *n*-butanol

C_{60} content (μM)	ξ-value (mV)	σ_{sc},-value (mS/cm)	L_{hd}-value (nm)	PDI-value
0	(-) 5.6	0.043	30.0	0.298
4.63	(-) 12.4	0.065	9.2	0.350
9.26	(-) 17.0	0.081	10.0	0.388
13.90	(-) 22.0	0.091	13.0	0.272
18.52	(-) 10.8	0.062	12.6	0.409
23.15	(-) 9.6	0.051	17.0	0.458

(N.B.: The samples were diluted five times in n-butanol before taking the readings)

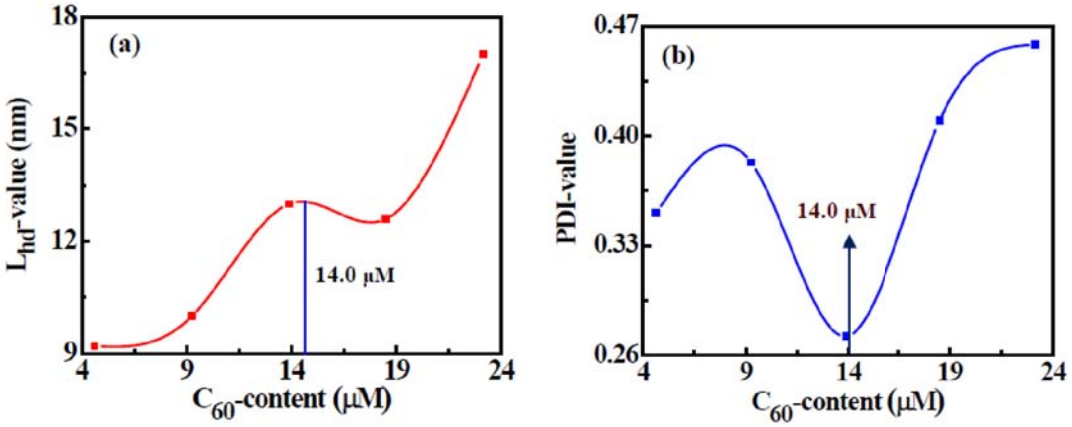

Figure 3. Variations in (a) average L_{hd}-value and (b) PDI-value in the C_{60}:PVP NFs with C_{60}-content prepared in 40.0 g/L PVP in *n*-butanol.

Furthermore, I studied the variations in L_{hd} and PDI values with C_{60}-content in the synthesized C_{60}:PVP NFs in *n*-butanol. As the results are plotted in Figure 3, both these physical parameters trace a nonlinear path with the C_{60} doping of a 40.0 g/L PVP in a solution in *n*-butanol over a wide region of 4–24 μM covered in this experiment. It is evident from the plot in Figure 3a that on increasing the C_{60}-content, the L_{hd}-value displays a peak in a percolation effect near 14.0 μM C_{60}. The C_{60}–content determines how it forms a C_{60}-PVP complex on reaction with exfoliated PVP molecules in a dilute liquid medium. Conversely, the PDI-value Vs C_{60}-content plot made in Figure 3b exhibits a sharp dip near the same value of 14.0 μM C_{60}. As a result, a minumium PDI-value of 0.272 is obtained in sample (d) and it implies that both the C_{60}-PVP and PVP entities are distributed reasonably uniformly in their effective sizes in the two distinct distribution bands in *n*-butanol. This results are differ from the observation of Alagrova et al. [18] that an average L_{hd}-value of C_{60} clusters in colloidal dispersions made in organic solvents such as toluene, benzene, xylene, chloroform, etc. does not changed much on varying the C_{60}-content. Though the reported PDI indices in all these dispersions were reasonably small below a 0.1 value, the L_{hd}-value was rather large lying between 207–240 nm when the C_{60}-content is increased from 0.001 to 0.02 g/L C_{60} (or 1.39 to 27.77 μM) without using a stabilizing agent. These L_{hd}-values are comparatively very large as compared our values estimated in the C_{60}:PVP NFs in *n*-butanol.

3.2 Zetapotential and surface conductivity of C_{60}:PVP NFs

I studied distribution of ξ-values in C_{60}:PVP NFs consisting of (a) 0, (b) 4.63, (c) 9.26, (d) 13.9, (e) 18.52, and (f) 23.15 μM C_{60} in 40.0 g/L PVP in *n*-butanol. As the experimental data could be collected only from reasonably dilute samples, I made samples dilute by 5–10 times from the parent samples in *n*-butanol (average 6.8 pH).

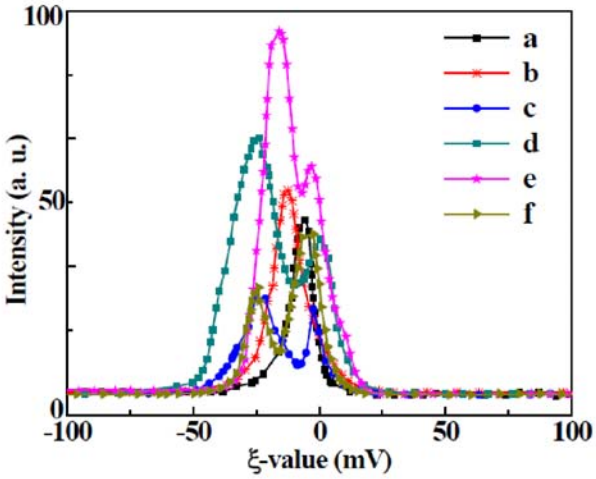

Figure 4. Distribution of ξ-values in C_{60}:PVP NFs consisting of (a) 0, (b) 4.63, (c) 9.26, (d) 13.9, (e) 18.52, and (f) 23.15 μM C_{60} along with 40.0 g/L PVP in *n*-butanol.

As the spectra are shown in Figure 4 for the various samples, a bare PVP solution in sample (a) exhibits a single sharp zeta band at an average ξ-value (-) 5.6 mV with fwhm ~9.1 mV and σ_{sc}-value 0.043 mS/cm in *n*-butanol at 6.8 pH. A negative ξ -value in the bare PVP molecules result from the presence of n-electrons on the >C–N and C=O sites over >N–C=O moieties in PVP molecules. Moreover, a merely 4.63 μM of C_{60} molecules when admixed to sample (a) causes a pretty broader zeta band of an average ξ-value increased to (-) 12.4 mV, with fwhm ~14.4 mV and an enhanced σ_{sc}-value to 0.065 mS/cm. As reported in articles [25-30], this type enhanced values in these two parameters are ascribed to accumulation of n-electrons of >N–C=O moieties from the PVP molecules on the C_{60} surface apparently in the form of a C_{60}:PVP charge transfer complex.

It is also observed from the spectra in Figure 4 that, as the C_{60} doping concentration reaches to a critical value 9.26 μM and above, two types of size distributions of the flocculates emerge in two distinct ξ-bands. Both the bands are prominent in sample (e) which contains 18.52 μM C_{60} molecules. A sample (f) having a still larger C_{60}-content of 23.15 μM displays two well-separated bands apart at (-) 2.2 and (-) 24.0 mV but of relatively poor intensities. The first band is rather stronger and sharing about 60 % integrated intensity. Primarily C_{60} molecules which are encapsulated in PVP molecules in a stable surface layer exhibit this specific band. The other band ascribes to PVP molecules which are merely dispersed via solvent *n*-butanol. An average ξ-value (-) 9.6 mV is estimated from a spectrum of a double band, with σ_{sc} = 0.051 mS/cm.

The values obtained for ξ and σ_{sc} in a bare 40.0 g/L PVP solution and that of reinforced with different C_{60} dosages in the forms of C_{60}:PVP NFs in *n*-butanol are given in Table 1. A comparison of the ξ-values in correlation to L_{hd} values in these samples suggests that a pretty large value, i.e. as much as (-) 22.0 mV, possibly arises as an effectively large number density is set-up of PVP modified C_{60} particles at an optimal doping of 13.9 μM C_{60}, which is the percolation threshold value. Eventually, such a sample shares an effectively large surface-interface area of large number of C_{60} particles so as they adsorb exfoliated PVP molecules in a concomitantly large number over them to give rise an effectively large number of n-electrons localized over the ">N-C=O" moieties of a PVP surface layer. This is what is required to promote an efficient electron transfer of the localized n-electrons from a PVP surface layer to the C_{60} core in a PVP surface modified C_{60} of small particles and/or joint C_{60}:PVP assemblies.

I also studied how the ξ and σ_{sc}-values vary in these C_{60}:PVP NFs with the C_{60}-content in an alcoholic medium. As depicted in Figure 5, both these parameters show two overlapping peaks, one near 5.5 μM C_{60} and other at 13.3 μM C_{60}, which acquires a relatively small viscosity with a reasonably decreased PDI (Table 1) in the C_{60}:PVP NFs.

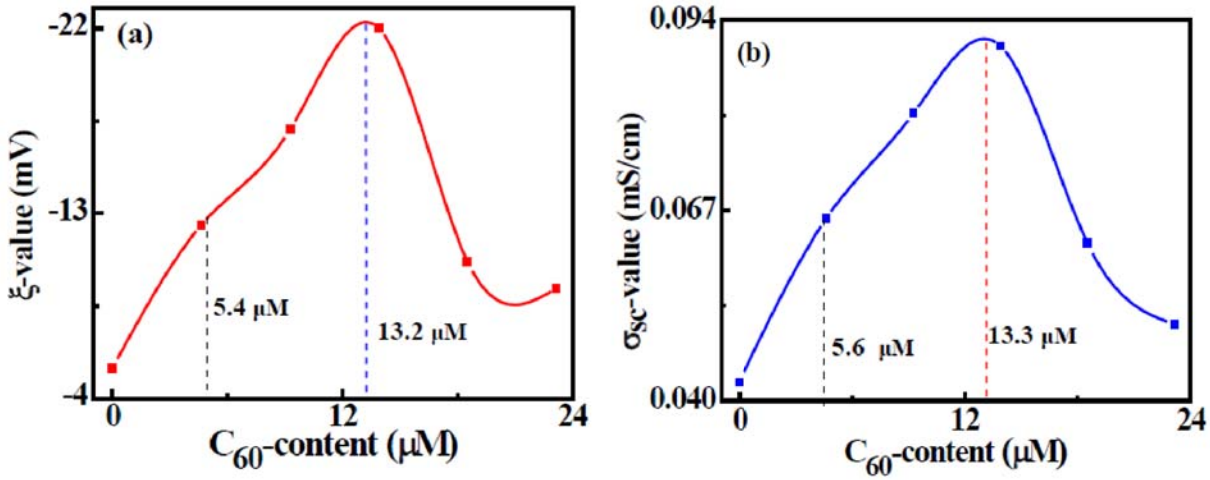

Figure 5. Variations in (a) ξ-value and (b) σ_{sc}-value in a bare 40.0 g/L PVP solution and that grafted with different C_{60} dosages in the forms of C_{60}: PVP NFs in *n*-butanol.

As a result, effectively large ξ and σ_{sc}-values have a correlation to a moderately viscous sample. Such a sample lets a light induced mechanical perturbation propagate through the sample. In the other wards, an exfoliated PVP molecule gets easily adsorbed on a C_{60} nanosurface via n-electron rich C–N and C=O sites in a PVP surface layer in a core-shell structure.

3.3 Thermal analysis of C_{60}:PVP nanocomposites

Figure 6 shows the TGA curves for (a) PVP without C_{60} and C_{60}:PVP nanocomposite films consisting of (b) 4.63, (c) 9.26, (d) 13.9, (e) 18.15, and (f) 23.15 μM C_{60}. From the Figure 6 it was observed that the onset temperatures of thermal degradation of C_{60}:PVP nanocomposite films were higher than that of pure PVP. For C_{60}:PVP nanocomposite films, it increases non-linearly with C_{60} content with a hump near 13.9 μM C_{60} (Figure 7a). The enhancement in the thermal stability of nanocomposite film is ascribed to the radical capturing ability of C_{60} [5-11].

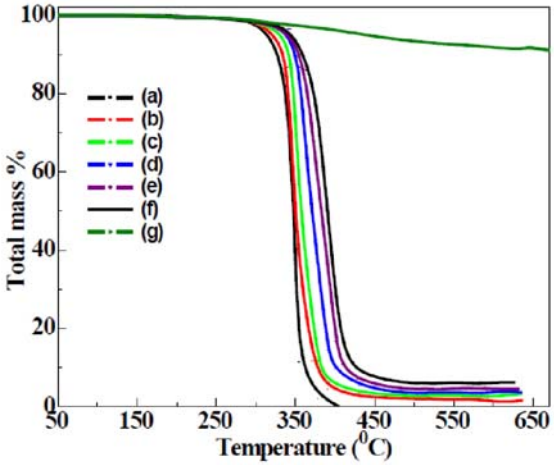

Figure 6. TGA curves for (a) PVP and PVP-C_{60} nanocomposites consisting of (b) 4.63, (c) 9.26, (d) 13.9, (e) 18.52, and (f) 23.15 μM C_{60}. 'g' is for C_{60} without PVP

The macroradicals which were usually obtained during the thermal degradation process are detained by C_{60} so that it restricts the thermal degradation of the polymer. In section 3.1, I report lowest PDI 0.272 for sample (d) consisting of 13.9 μM C_{60}. This shows that in this sample C_{60} molecules are uniformly distributed in PVP matrix and this is reflected as a crest near 13.9 μM C_{60} in Figure 7a. The microscopic image also supports our observation (see Figure 8). In a report, Fernandes et al. [8] have reported an improvement in the thermo-oxidative stability of the functionalized C_{60}/PS composites compared to the unfunctionalized C_{60} composites and they attributed it to the fact that functionalized C_{60} disperses better in a polymer matrix than C_{60}. I also studied the % total residual mass at 550 ^{0}C as a function of C_{60} content (Figure 7b). The char residue % at this temperature is found to be more for the sample containing more carbon materials i.e., C_{60}. The plot shows that two parameters vary linearly with each other and reveals that thermal stability of nanocomposites depends on the content of cross-linkers i.e., the carbon materials.

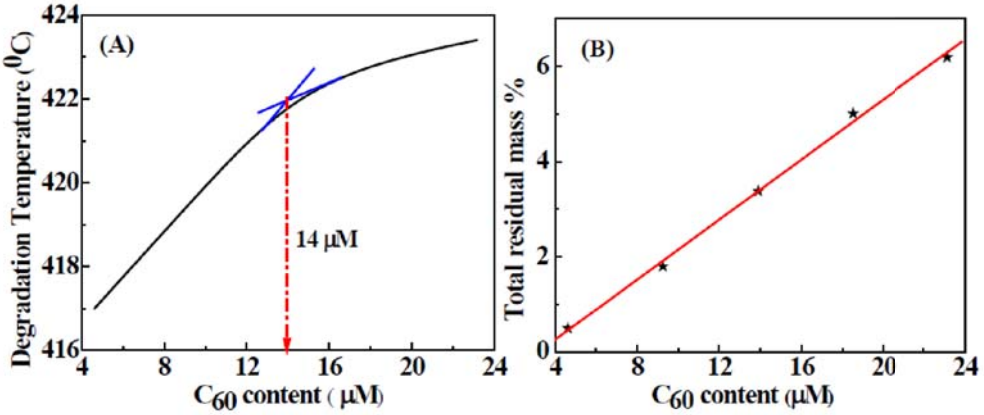

Figure 7. Variation of (A) degradation temperature and (B) total residual mass % against C_{60} content in PVP-C_{60} nanocomposite films.

3.4 Microstructures of C_{60}:PVP nanocomposite films

Figure 8 shows TEM images obtained for C_{60}:PVP nanocomposite films consisting of (a) 4.63, (b) 9.26, (c) 13.9, and (d) 23.15 μM C_{60}. Assemblies of the C_{60} NPs capped by PVP of near spheroids of 10–20 nm diameters are by and large shown in different polygons.

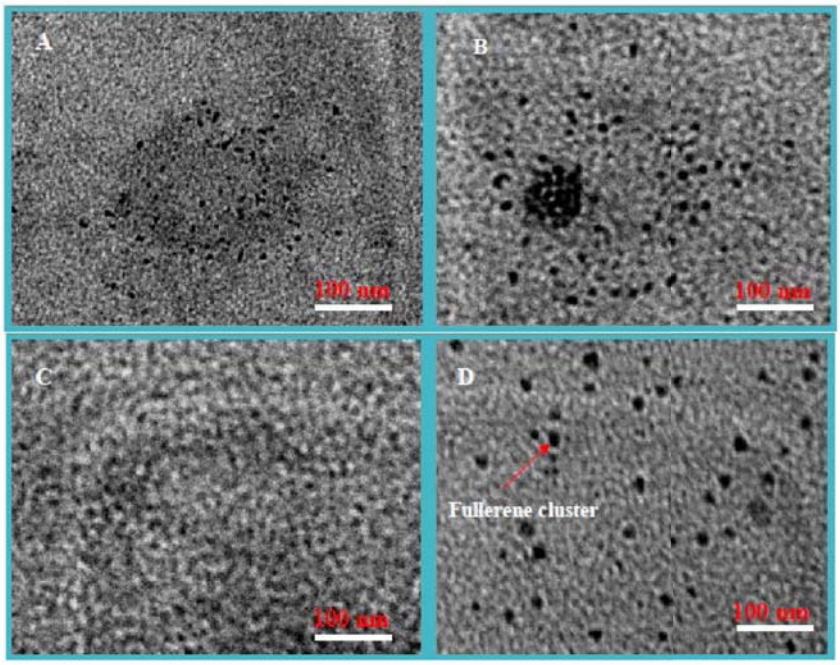

Figure 8. TEM images of PVP-C_{60} nanocomposite films consisting of (a) 4.63, (b) 9.26, (c) 13.9, and (d) (d) 23.15 μM C_{60}.

The C_{60} cluster size increases from 10 nm in sample (a) to nearly 20 nm in sample (d) due to a relative decrease in the encapsulant PVP content. The micrograph for the sample consisting of 13.9 μM C_{60} which shows a uniform distribution of C_{60} NPs in the PVP matrix possess highest degradation temperature (~ 422 ^{0}C) amongst all samples (Figure 8c) owing to possession of suitable network structure.

4.0 Conclusion

From the DLS study I found that an average L_{hd}-value of 9.2 nm for a C_{60}:PVP NF consisting of 4.63 μM C_{60} has grown-up significantly to 17.0 nm when the dopant concentration has increased to 23.15 μM C_{60}. Both L_{hd} and PDI values sketch a non-linear path with the C_{60} doping in the NFs over a wide range of 4–24 μM C_{60} covered in this experiment. In comparison to a negative ξ-value of (-) 5.6 mV with fwhm ~9.1 mV and σ_{sc}-value 0.043 mS/cm in the bare PVP molecules, a relatively broader zeta band of an average ξ-value increased to (-) 12.4 mV, with fwhm ~14.4 mV and an enhanced σ_{sc}-value to 0.065 mS/cm in a C_{60}:PVP NF with 4.63 μM C_{60} reveals accumulation of n-electrons of >N–C=O moieties from the PVP molecules on the C_{60} surface in C_{60}:PVP charge transfer complex. Considerably increase in the thermal stability of nanocomposite films is credited to C_{60} for its excellent radical capturing ability.

Acknowledgements

I highly acknowledge the support of Silicon Institute of Technology, Bhubaneswar, India in carrying out this work.

References

1. A, Dasari, Z.Z. Yu, Y.W. Mai, 2016, *Polymer Nanocomposites: Towards Multi-Functionality.* Springer.
2. P.M. Visakh, B. N. Olga, 2015, *"Thermal Degradation of Polymer Blends, Composites and Nanocomposites." In Thermal Degradation of Polymer Blends, Composites and Nanocomposites*, Pp. 1-16. Springer International Publishing.
3. M. Prato, 2009, *Fullerene polymers: synthesis, properties and applications*. Eds. N. Martín, F. Giacalone, John Wiley & Sons.
4. C. N. Kramer, ed. 2007, *Fullerene Research Advances.* Nova Publishers.
5. L. Zhao, Z. Guo, S. Ran, Z. Cao, 2014, Fang, *Journal of Thermal Analysis and Calorimetry*, Vol. *115, No.* 2, Pp.1235-1244.
6. H. Gaspar, L. Fernandes, P. Pereira, G. Bernardo, 2015, *Polymer Bulletin*, *Vol.* 7, Pp.1775-1786.
7. R. Katiyar, D.S. Bag, I. Nigam, 2013, *Thermochimica Acta*, 2013, *557*, pp.55-60.
8. L. Fernandes, H. Gaspar, G. Bernardo, *Polymer Testing*, 2014, Vol. *40*, Pp.63-69.
9. K. Kokubo, R. Takahashi, M. Kato, A. Harada, T. Noguchi, T. Oshima, 2016, *Polymer Composites*. Vol. 37, No. 4, Pp.1143-1151.
10. P.A. Song, Y. Zhu, L. Tong, Z. Fang, 2008, *Nanotechnology*, Vol. *19*, No. 22, p. 225707.
11. V.V. Zuev, F. Bertini, G. Audisio, 2005, *Polymer degradation and stability*,Vol. *90*, No.1, Pp.28-33.
12. J.Y. Lee, Y. Liao, R. Nagahata, S. Horiuchi, 2006, *Polymer*, Vol. *47*, No. 23, Pp.7970-7979.
13. T. Cosgrove, 2010, *Colloid science: Principle, methods, and applications*, Wiley.
14. R. J. Hunter, 1998, *Zetapotential in colloid science: Principles and applications*, Academic Press, UK.
15. K. Rahme, L. Chen, R.G. Hobbs, M.A. Morris, C. O'Driscoll, J.D. Holmes, 2013, *Rsc Advances*, Vol. *3*, No.17, Pp.6085-6094.
16. W. Brown, 1993, *Dynamic Light Scattering: The Method and some Applications*, New York: Claredon.
17. B.J. Berne, R. Pecora, 2003, *Dynamic Light Scattering: with Applications to Chemistry, Biology, and Physics*, Dover publications,
18. R.G. Alargova, S. Deguchi, K. Tsujii, 2001, *Journal of the American Chemical Society*, Vol. *123, No.* 43, Pp. 10460-10467.
19. V.R. Chaudhari, S.K. Haram, S.K. Kulshreshtha, J.R., Bellare, P.A. Hassan, 2007, *Colloids and Surfaces A: Physicochemical and Engineering Aspects*, 2007, Vol. *301, No.* 1, Pp. 475-480.
20. G. Mountrichas, S. Pispas, E. Xenogiannopoulou, P. Aloukos, S. Couris, 2007, *The Journal of Physical Chemistry B*, 2007,Vol. *111, No.* 17, Pp. 4315-4319.
21. N.P. Yevlampieva, S.K. Filippov, T.S. Dmitrieva, I.I. Zaitseva, E.Y. Melenevskaya, O.V. Nazarova, E.I. Ryumtsev, 2007, *Polymer Science Series A*, *Vol. 49, No.* 6, Pp. 642-650.
22. Z. Wang, B. Tan, I. Hussain, N. Schaeffer, M.F. Wyatt, M. Brust, A.I. Cooper, 2007, *Langmuir*, Vol. *23, No.* 2, Pp. 885-895.
23. A. Mishra, A., S. Ram, G. Ghosh, 2009, *The Journal of Physical Chemistry C*, Vol. *113, No.* 17, Pp.6976-6982.
24. M. Behera, 2015, *International Nano Letters*, Vol. *5, No.* 3, Pp.161-169.
25. M. Behera, S. Ram, 2015, *Applied Nanoscience*, 2014, Vol. *4, No.*2, Pp. 247-254.
26. M. Behera, S. Ram, 2013, *International Nano Letters*, Vol. *3*, No. 1, p. 1.
27. M. Behera, S. Ram, 2013, *Applied Nanoscience*, Vol. *3, No.* 1, Pp. 83-87.

28. M. Behera, S. Ram, 2015, *Fullerenes, Nanotubes and Carbon Nanostructures*, Vol. *23*, No. 10, Pp. 906-916.
29. M. Behera, 2015, *Research Journal of Nanoscience and Nanotechnology*, Vol. 5, Pp. 60-73.
30. M. Behera, S. Ram, 2016, *Plasmonics*, Vol. 14, No. 4, pp. 1057-1065.